© 2014. Published by The Company of Biologists Ltd | Journal of Cell Science (2014) 127, 1079–1091 doi:10.1242/jcs.142075

RESEARCH ARTICLE

TGF-β-induced differentiation into myofibroblasts involves specific regulation of two MKL1 isoforms

Matthias A. Scharenberg[1,2], Benjamin E. Pippenger[3], Ragna Sack[1], Dominik Zingg[1], Jacqueline Ferralli[1], Susanne Schenk[1,4], Ivan Martin[2] and Ruth Chiquet-Ehrismann[1,2,*]

ABSTRACT

Cellular transformation into myofibroblasts is a central physiological process enabling tissue repair. Its deregulation promotes fibrosis and carcinogenesis. TGF-β is the main inducer of the contractile gene program that drives myofibroblast differentiation from various precursor cell types. Crucial regulators of this transcriptional program are serum response factor (SRF) and its cofactor MKL1 (also known as MRTF-A). However, the exact mechanism of the crosstalk between TGF-β signaling and MKL1 remains unclear. Here, we report the discovery of a novel MKL1 variant/isoform, MKL1_S, transcribed from an alternative promoter and uncover a novel translation start for the published human isoform, MKL1_L. Using a human adipose-derived mesenchymal stem cell differentiation model, we show that TGF-β specifically upregulates MKL1_S during the initial phase of myofibroblast differentiation. We identified a functional N-terminal motif in MKL1_S that allows specific induction of a group of genes including the extracellular matrix (ECM) modifiers MMP16 and SPOCK3/testican-3. We propose that TGF-β-mediated induction of MKL1_S initiates progression to later stages of differentiation towards a stationary myofibroblast.

KEY WORDS: Myofibroblast differentiation, MKL1, Gene regulation, MRTF-A

INTRODUCTION

Differentiation of a variety of cell types into myofibroblasts defines a major physiological process that facilitates wound healing and tissue repair. Tissue damage drives the transformation of diverse quiescent tissue-resident cells or invading circulating cells into a mesenchymal proliferative and migratory phenotype (termed proto-myofibroblast) involving the formation of smooth muscle α-actin (SMA)-negative stress fibers (Tomasek et al., 2002). The proto-myofibroblasts expand towards the wound where they develop a contractile phenotype with characteristic SMA-positive stress fibers typical of mature myofibroblasts. Myofibroblasts produce large amounts of extracellular matrix (ECM) proteins, such as type I collagen, fibronectin, tenascin-C and matrix metalloproteinases (MMPs), contributing to the replacement of the granulation tissue and the scarring of the wound (Sarrazy et al., 2011). Organ fibrosis and fibrotic scarring arise from excessive extracellular matrix deposition by persistent myofibroblasts, which can occur after tissue damage, but can also occur in the context of chronic inflammation and ageing, as well as in cancer stroma (Hinz et al., 2012). Fibrosis causes functional impairment of many organs and therefore constitutes a major health problem.

In both tissue repair and tumorigenesis, TGF-β represents the prototypic inducer of myofibroblast differentiation from all precursor cell types. Therefore, interfering with TGF-β signaling currently poses one of the main therapeutic approaches for fibrosis and cancer (Hinz et al., 2012). The Rho–actin–MKL1–SRF and Smad signaling pathways have been identified as major drivers to elicit the contractile gene expression program. Key regulators of these pathways are the transcription factors megakaryoblastic leukemia 1 (MKL1)/myocardin-related transcription factor-A (MRTF-A) and Smad3, respectively (Charbonney et al., 2011; Crider et al., 2011; Small, 2012). Rho-dependent association of serum response factor (SRF) with members of the MRTF family has recently been described as a mechano- and growth-factor-sensitive pathway that regulates expression of many cytoskeletal, ECM and contractile proteins (Wang et al., 2001; Wang et al., 2002). Its activity is directly dependent on the polymerization status of the actin cytoskeleton. In quiescent cells, binding to G-actin renders MKL1 inactive, keeping it mainly in the cytosol. Rearrangement of the actin cytoskeleton in response to stimulation from the extracellular environment depletes G-actin and liberates MKL1, which can accumulate in the nucleus to activate SRF-mediated transcription (Miralles et al., 2003).

Common protein databases at the time of submission of this article listed human MKL1 (Q969V6; NP_065882.1; CAG30408.1) as a 931-amino-acid protein with translation starting at the first ATG start codon. This protein would contain only two actin-binding RPEL motifs, despite a third highly conserved RPEL motif being encoded within its 5′ untranslated region. Therefore, Miralles and colleagues (Miralles et al., 2003) have suggested for an orthologous mouse MKL1 transcript that translation starts at an upstream CTG (Leu-92), embedding the RPEL1 motif within the coding sequence. Here, we characterized human MKL1 in different cell types and tissues and discovered that two human *MKL1* mRNAs are transcribed from alternative promoters. This results in two isoforms that differ in their N-terminal domains as well as in their functions. We identified the specific induction of a group of genes by the shorter MKL1_S isoform. This isoform is strongly upregulated during the initial phase of TGF-β-induced differentiation of human

[1]Friedrich Miescher Institute for Biomedical Research, Department of Mechanisms of Cancer, Maulbeerstrasse 66, CH-4058, Basel, Switzerland. [2]University of Basel, Faculty of Sciences, CH-4056, Basel, Switzerland. [3]University Hospital Basel, Departments of Surgery and Biomedicine, Hebelstrasse 20, CH-4031, Basel, Switzerland. [4]Pharmazentrum Basel, Division of Pharmaceutical Technology, Klingelbergstrasse 50, CH-4056 Basel, Switzerland.

*Author for correspondence (ruth.chiquet@fmi.ch)

Received 2 September 2013; Accepted 4 December 2013

Journal of Cell Science (2014) 127, 1079–1091 doi:10.1242/jcs.142075

adipose tissue-derived stem cells (hASCs) into myofibroblasts, suggesting that there is a specific function of its target genes in subsequent steps of differentiation.

RESULTS

Translation of the published human *MKL1* mRNA starts at an upstream GTG codon

To identify the translation start of human MKL1, we expressed a human cDNA construct comprising the full 5′UTR and the sequence coding for the N-terminal half of the published MKL1 protein (5′UTR-ΔC) in HEK293 cells and compared its size to the corresponding construct starting at the published ATG (ATG-ΔC). Only a minor product was found to co-migrate with ATG-ΔC and the main translation product migrated more slowly, indicating an upstream translation start (Fig. 1A). To identify its exact position, we purified MKL1 that was translated in HEK293 cells from a 5′UTR-full length MKL1 construct by antibody affinity chromatography. Using endoproteinase AspN cleavage and detection of peptides by liquid chromatography (LC)-mass spectrometry (MS), we achieved a full coverage of the in-frame translated 5′UTR of MKL1. The most N-terminal sequence that we identified is preceded by a putative GTG start codon, which would normally code for a valine at position −100 of the published ATG/Met start (Fig. 1B). Given that cleavage of the initiating amino acid is a common mechanism, this GTG was considered as the candidate start codon. By aligning the human 5′UTR nucleotide sequence to that from other species, this GTG codon depicts the most upstream putative start codon that is conserved in mouse and *Xenopus* MKL1 (Fig. 1C). In addition, with a G in position +4 and a purine base at −3 this nucleotide is flanked by a strong Kozak consensus sequence (Kozak, 1989), which is the main requirement for a GTG to serve as an unusual start codon. To experimentally test the function of this GTG as the translation start, we introduced the mutations into the 5′UTR-full length MKL1 construct (Fig. 1D). Introduction of the more potent ATG start codon into this context increased translation efficiency, and the resulting product migrated at the same position as from the GTG construct and the endogenous protein.

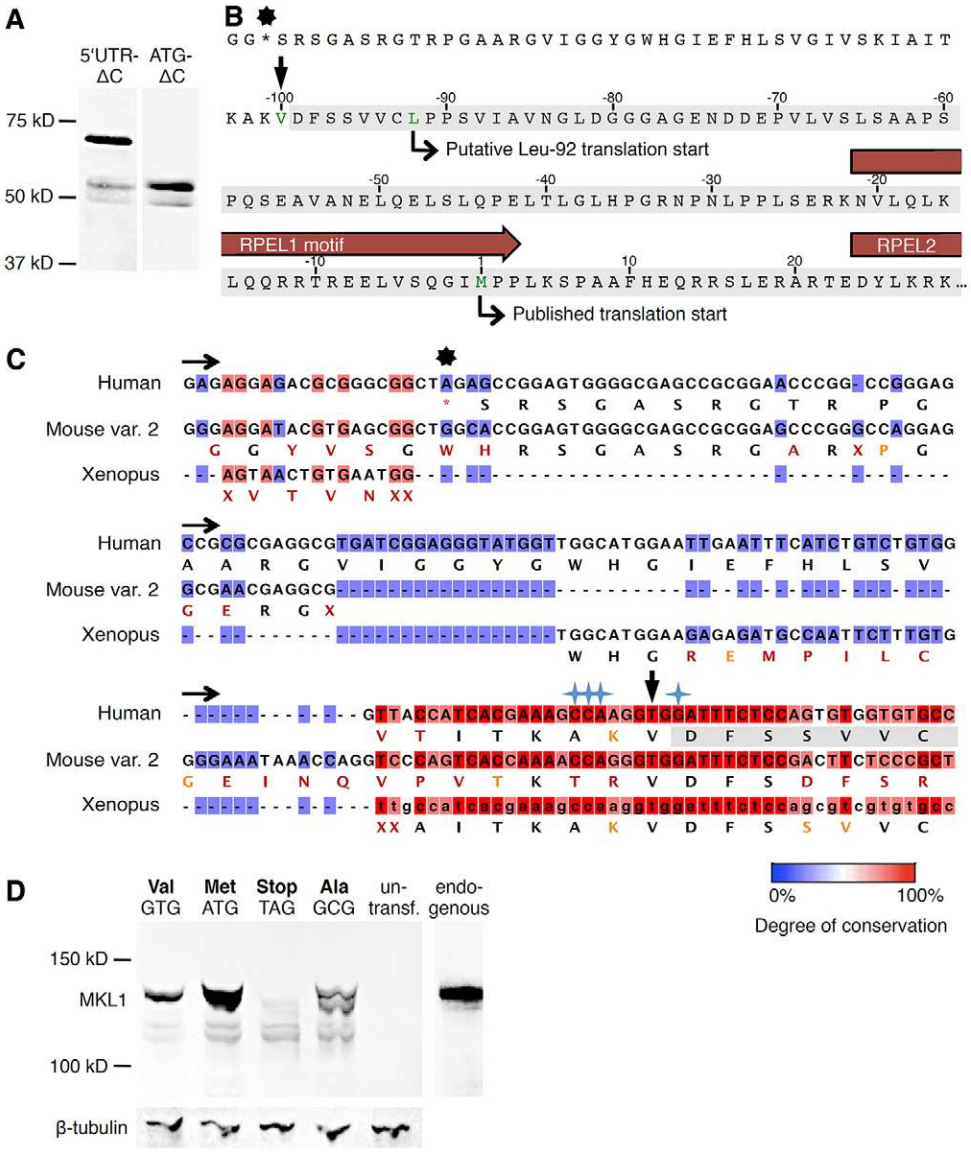

Fig. 1. Identification of an unusual translation start in the published human MKL1. (A) ATG-ΔC and 5′UTR-ΔC constructs were overexpressed in HEK293 cells, and MKL1 was detected by immunoblotting with anti-MKL1 total mAb. (B) Human 5′UTR-full-length MKL1 was overexpressed in HEK293 cells, the translated MKL1 was affinity purified, and the major product digested with AspN. Peptides were identified by LC-MS. Highlighted in gray, peptide coverage; black star, in-frame stop codon; green letters, suggested ATG, CTG or GTG translation initiation codons (coding for M, L and V, respectively); vertical arrow, putative GTG/Val-100 start. (C) Alignment of the human MKL1 5′UTR region with those of mouse (variant 2) and *Xenopus*. Horizontal arrows: 5′ to 3′ direction; black star, in-frame stop codon; vertical arrow, suggested GTG/Val-100 start; blue 4-point star, nucleotides complying with the Kozak consensus sequence. (D) Point mutations targeting the suggested GTG/Val-100 start codon were introduced into the construct shown in A, the resulting constructs were transiently overexpressed in HEK293 cells and MKL1 was detected by immunoblotting with anti-MKL1 total mAb. Endogenous human MKL1 was purified from untransfected (Untransf.) HEK293 cells as described in B.

Replacing the GTG start codon with GCG (Ala) greatly diminished translation and resulted in two different translation products, proving the importance of the GTG/Val-100 codon as the translation initiation codon of human MKL1. Finally, introduction of a stop codon abolished translation most efficiently, excluding the existence of further downstream translation starts. The eight additional amino acids that are included with the GTG (Val-100) translation start, but are not present with the CTG/Leu-92 start, are predicted to form two out of four β-strands within the N-terminal 36-amino-acid stretch (supplementary material Fig. S1A).

Human cells express a second shorter MKL1 isoform

To investigate endogenous MKL1 transcripts in human tissues we performed 5′ rapid amplification of cDNA ends (RACE) on total RNA from fetal and adult brain extracts, amplifying the region upstream of the published ATG start codon (Fig. 2A). Interestingly, we detected two major products of different sizes. Nucleotide sequencing revealed the expression of a second human transcript (for sequence see supplementary material Fig. S1B) homologous in sequence to the mouse MKL1 variant 1 (NM_153049.2). An alignment with the human genome reveals that this variant has a single alternative exon between the previously known exons 3 and 4. This novel exon represents an alternative 5′ end of the MKL1-encoding gene and thus implies the existence of an alternative promoter for this transcript (Fig. 2B). The new exon contains an in-frame ATG start codon. Thus, translation of this transcript is expected to yield a second MKL1 isoform that we termed MKL1_S (S for short), because it is shorter than the MKL1_L (L for long) isoform derived from the GTG/Leu-100 start of the published mRNA. MKL1_S carries a stretch of only 15 variant-specific amino acids at its N-terminus, whereas MKL1_L has a long tail of 80 variant-specific amino acids. Both isoforms are otherwise identical and both of them harbor all three RPEL repeats. To investigate whether the two MKL1 isoforms are indeed expressed in human cells at a protein level, we generated two monoclonal antibodies, one detecting a region of human MKL1 that is shared by both isoforms (detecting 'MKL1 total') and one that specifically recognizes the N-terminus of the novel MKL1_S. Endogenous MKL1 proteins were enriched by affinity purification from whole-cell extracts of U343MG glioblastoma cells using the antibody against MKL1 total. As shown in Fig. 2C, two distinct MKL1 isoforms could be detected, which corresponded in size with the overexpressed proteins translated from 5′UTR-full length constructs of the two MKL1 transcripts. Using the MKL1_S-specific antibody we confirmed that the observed lower band indeed constituted the novel isoform MKL1_S (Fig. 2C). No protein band of the size of the published ATG/Met start protein (smaller than MKL1_S) was detected, implying that MKL1_L and MKL1_S identified in our experiments are the main isoforms expressed in human cells. To assess the expression patterns of both isoforms in different human cells and tissues, we performed quantitative RT-PCR (qPCR) analysis with primers specific for each isoform (Fig. 2D). As estimated from the Ct values, MKL1_L was the major isoform in most of the cell types and tissues analyzed. MKL1_L expression levels were comparable in all samples, whereas MKL1_S levels varied greatly. In the majority of samples MKL1_S was expressed at a very low level, within a relative range of 1- to 20-fold above the lowest expressing cell line. However, a group of cell lines and tissues, including fetal and adult brain, expressed MKL1_S at much higher levels. For this group, the relative difference in expression of MKL1_S spanned 2 to 3 orders of magnitude compared to the lowest expressing cell line. Primary ASCs showed the highest expression of MKL1_S, which was $\sim 4\times10^3$-fold higher than that of the anaplastic astrocytoma cell line LN319. Notably, the purification of the endogenous protein isoforms from U343MG cells in Fig. 2C illustrates that even in cells that belong to the group with high relative MKL1_S expression (Fig. 2D), protein levels were lower than those of MKL1_L.

MKL1_L and MKL1_S show similar SRF-dependent transcriptional activities, responsiveness to Rho and nuclear translocation

To assess whether the different N-termini of the two MKL1 isoforms result in differential transcriptional activities, Rho-responsiveness or nuclear translocation, we investigated the transactivation of SRF and the kinetics of MKL1 isoform nuclear accumulation after stimulation of the Rho–actin–MKL1 pathway. Promoter–reporter assays after co-transfection of different MKL1 constructs with a 3×CArG box promoter construct are shown in Fig. 2E. We did not observe any difference in activation of the SRF reporter construct by MKL1 constructs harboring the different translation starts. However, the ability to induce SRF activity was strongly impaired in a C-terminally truncated construct lacking the transactivation domain.

MKL1 staining in HEK293 cells that overexpress either of the two isoforms revealed comparable nuclear accumulation kinetics for MKL1_L and MKL1_S after stimulation with fetal calf serum (FCS), lysophosphatidic acid (LPA) and cytochalasin D (Fig. 3). With FCS and LPA, two classical activators of the Rho–actin–MKL1 pathway, nuclear accumulation of each MKL1 isoform was already visible after 5 min of treatment (Fig. 3A,B). In the case of FCS treatment, ~80% of cells showed nuclear accumulation of each isoform and the peak was already reached after 5 min. With LPA we observed a more pronounced nuclear accumulation for MKL1_S than for MKL1_L, which increased within 60 min to ~75% cells for MKL1_S and 60% cells for MKL1_L. However, this difference was not statistically significant. To assess possible differences in nuclear import or export rates between the two isoforms, we treated the cells with the actin polymerization inhibitor cytochalasin D. This drug binds to G-actin and thereby liberates MKL1 from actin inhibition. Independent of the MKL1 isoform, 100% of cells showed nuclear MKL1 localization after 5–60 min of cytochalasin D treatment (Fig. 3C). Nuclear translocation of MKL1 isoforms was also confirmed by cell fractionation. Cells were harvested 5 min after treatment with FCS, LPA or cytochalasin D, and cytoplasmic and nuclear extracts were prepared. Immunoblot analysis of these extracts revealed nuclear MKL1_S and MKL1_L in cells stimulated with either of these agents but not in untreated cells (supplementary material Fig. S3). We therefore conclude that despite the small differences after LPA stimulation, MKL1_L and MKL1_S exhibit similar SRF-dependent transcriptional activities, Rho-responsiveness and nuclear import and export efficiencies.

The initial phase of TGF-β1-induced myofibroblastic differentiation involves specific upregulation of MKL1_S expression

In order to study MKL1 isoform expression during myofibroblast differentiation, we used primary hASCs, which can be induced to differentiate into myofibroblasts by the addition of TGF-β1 (Kakudo et al., 2012). We isolated the stromal vascular fraction (SVF) of cells from patient adipose tissue, which was confirmed

Journal of Cell Science (2014) 127, 1079–1091 doi:10.1242/jcs.142075

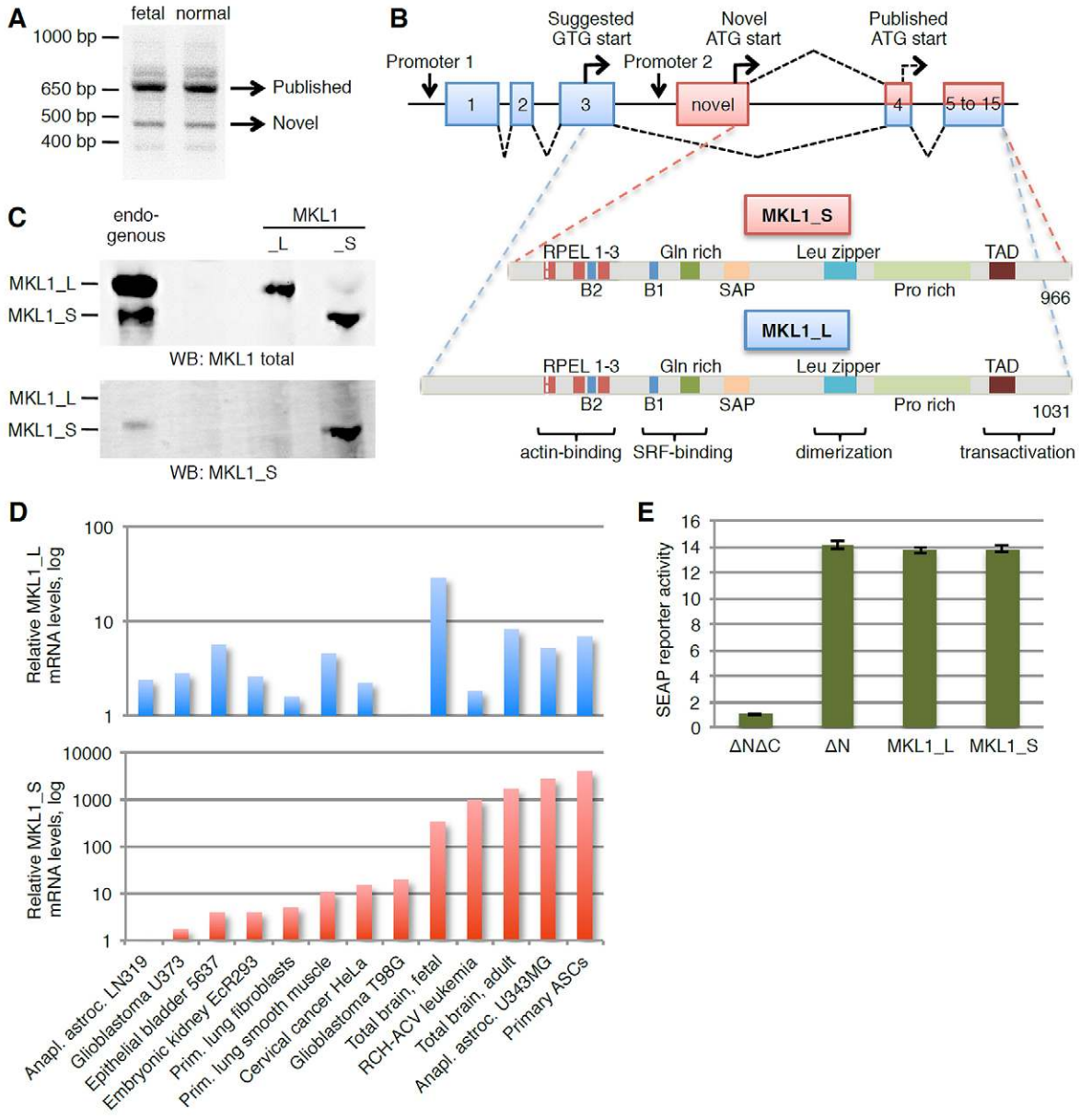

Fig. 2. Identification of a second human MKL1 isoform. (A) 5′RACE on total RNA from human brain extracts. The MKL1 5′UTR region was amplified using a reverse primer located 3′ of the published ATG/Met start codon and the main products were sequenced. (B) Alignment of the two MKL1 transcripts with the human genome. An alternative exon with an upstream ATG/Met start codon results in the translation of the shorter MKL1_S isoform. Translation starting at the suggested GTG/Val-100 codon of the published transcript results in the longer MKL1_L isoform. The sequences C-terminal of the white dashed line are identical in the two isoforms. B, basic motif; TAD, transactivation domain. (C) Western blot detection of both human isoforms at the protein level. Detection on the same membrane was achieved by two-channel detection of two antibodies with the LI-COR Odyssey system. Left: endogenous MKL1 was affinity purified from U343MG glioblastoma cell extract with the anti-MKL1 total mAb. Right: cell extracts from HEK293 cells stably overexpressing either MKL1_L or MKL1_S. (D) Total RNAs from human cell lines and tissues were subjected to quantitative RT-PCR analysis with primers specific for each MKL1 isoform. Isoform levels relative to *GAPDH* were calculated by using the relative standard curve method. Averages of triplicate measurements from single batches of RNA are shown (n=1). Anapl. astroc., anaplastic astrocytoma; prim., primary. (E) SEAP (for secreted alkaline phosphatase) promoter–reporter assay. HEK293 cells were transiently co-transfected with an MKL1 construct and a 3×CArG box SEAP reporter construct. 18 h after LPA stimulation the amount of secreted alkaline phosphatase was determined. Constructs: ΔNΔC, published ATG/Met start (ΔN) with the C-terminal half of MKL1 missing (ΔC); Δ*N*, published ATG/Met start full length MKL1; MKL1_L, 5′UTR-full length MKL1_L; MKL1_S, 5′UTR-full length MKL1_S. Data are represented as mean±s.d. (n=4).

to contain a large proportion of mesenchymal stems cells (MSCs) expressing the mesenchymal markers CD73, CD90 and CD105 (Fig. 4A). Adherent cells were expanded to obtain a population of primary hASCs. Treatment of these cells with serum-free medium containing 2 ng/ml TGF-β1 for 96 h clearly induced their differentiation, as documented by their change in morphology and the expression of SMA-positive stress fibers compared to cells incubated with the control medium (Fig. 4B). We analyzed the transcript levels of several myofibroblast markers and the MKL1 isoforms 24 h and 96 h after TGF-β1-induced differentiation. A significant increase of the prototypic marker of differentiated myofibroblasts SMA (*ACTA2*) and other

Journal of Cell Science (2014) 127, 1079–1091 doi:10.1242/jcs.142075

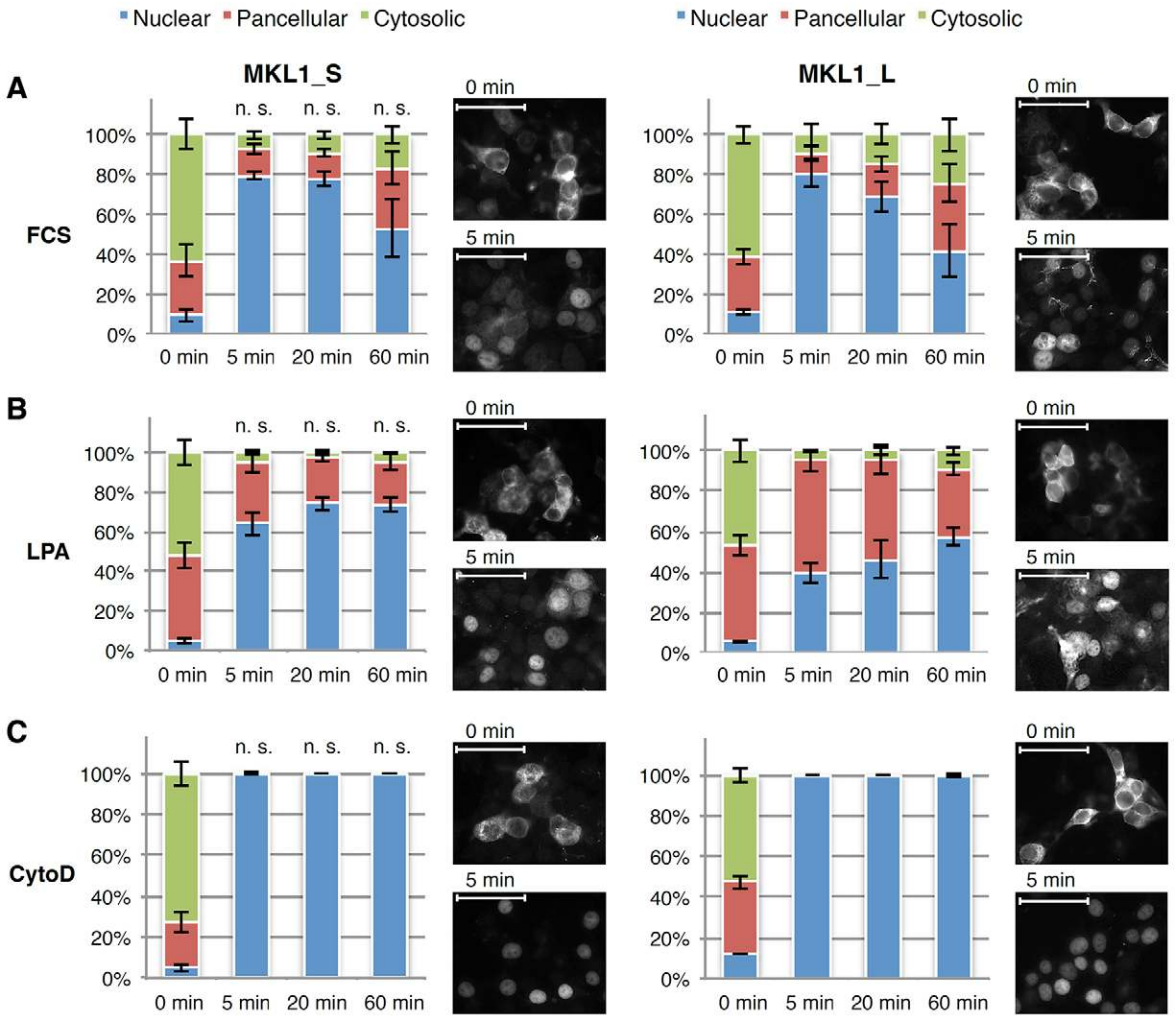

Fig. 3. MKL1_S and MKL1_L show similar nuclear translocation properties. HEK293 cells stably overexpressing 5′UTR-full length MKL1_S or MKL1_L constructs were starved and treated with (A) 15% FCS, (B) 50 μM LPA, or (C) 2 μM Cytochalasin D (CytoD) for 0–60 min. Cells were stained with the anti-MKL1 total mAb and fluorescence images were taken. Overexpressing cells were classified according to their predominant subcellular localization of MKL1 into 'nuclear', 'pancellular' or 'cytosolic'. At least 30 cells were counted in each of three independent experiments for each treatment at each time point. The percentage of cells per category was calculated and data are represented as mean±s.e.m. (n=3). n.s., not significant in comparison to MKL1_L under the same conditions in an unpaired Student's t-test. Scale bars: 50 μm.

contractility-promoting genes such as calponin-1 (*CNN1*) and SM22α (*TAGLN*), as well as tenascin-C (*TNC*) was observed compared to untreated cells. (Fig. 4C). As reported by others (Mihira et al., 2012; Minami et al., 2012; Sandbo et al., 2011), we also observed an increase in total MKL1 levels compared to control cells (Fig. 4D). However, the use of isoform-specific primers revealed that the expression of the major human isoform MKL1_L did not change significantly in response to TGF-β1, whereas expression of the novel isoform MKL1_S was induced more than 10-fold within 24 h of differentiation and remained high after 96 h (Fig. 4D). The small effect of this strong MKL1_S induction on total MKL1 levels can be explained by the fact that MKL1_S basal levels were clearly lower than MKL1_L basal levels in the undifferentiated hASCs (estimated from the Ct values). Our data suggest that the known increase of MKL1 expression during TGF-β-induced myofibroblast differentiation is mainly driven by a strong induction of MKL1_S transcription. Thus, TGF-β1 seems to be a potent isoform-specific inducer of MKL1_S, and TGF-β1-induced differentiation of hASCs into myofibroblasts involves a strong upregulation of the MKL1_S mRNA level during the initial 24 h of differentiation.

MKL1_S upregulation is specific for TGF-β1-induced differentiation

To assess whether MKL1_S upregulation constitutes a general mechanism during hASC differentiation, we used other media to differentiate hASCs/MSCs into different cell types. With chondrogenic medium containing TGF-β1 at a concentration of 10 ng/ml, we obtained a comparably strong upregulation of MKL1_S after 24 h and 96 h as with TGF-β1 alone (Fig. 4E). LPA has been reported to induce expression of total MKL1 in hASCs (Jeon et al., 2010; Jeon et al., 2008a), but in our experiments using 5 μM LPA we neither observed an upregulation of total MKL1 transcript levels compared to control cells, nor of one of the MKL1 isoforms alone (Fig. 4F). Likewise, the stimulation of hASCs to differentiate towards a smooth muscle phenotype using 2 μM sphingosylphosphorylcholine (SPC) (Jeon et al., 2008b) or 5% uniaxial cyclic strain (Kurpinski et al., 2009)

Journal of Cell Science (2014) 127, 1079–1091 doi:10.1242/jcs.142075

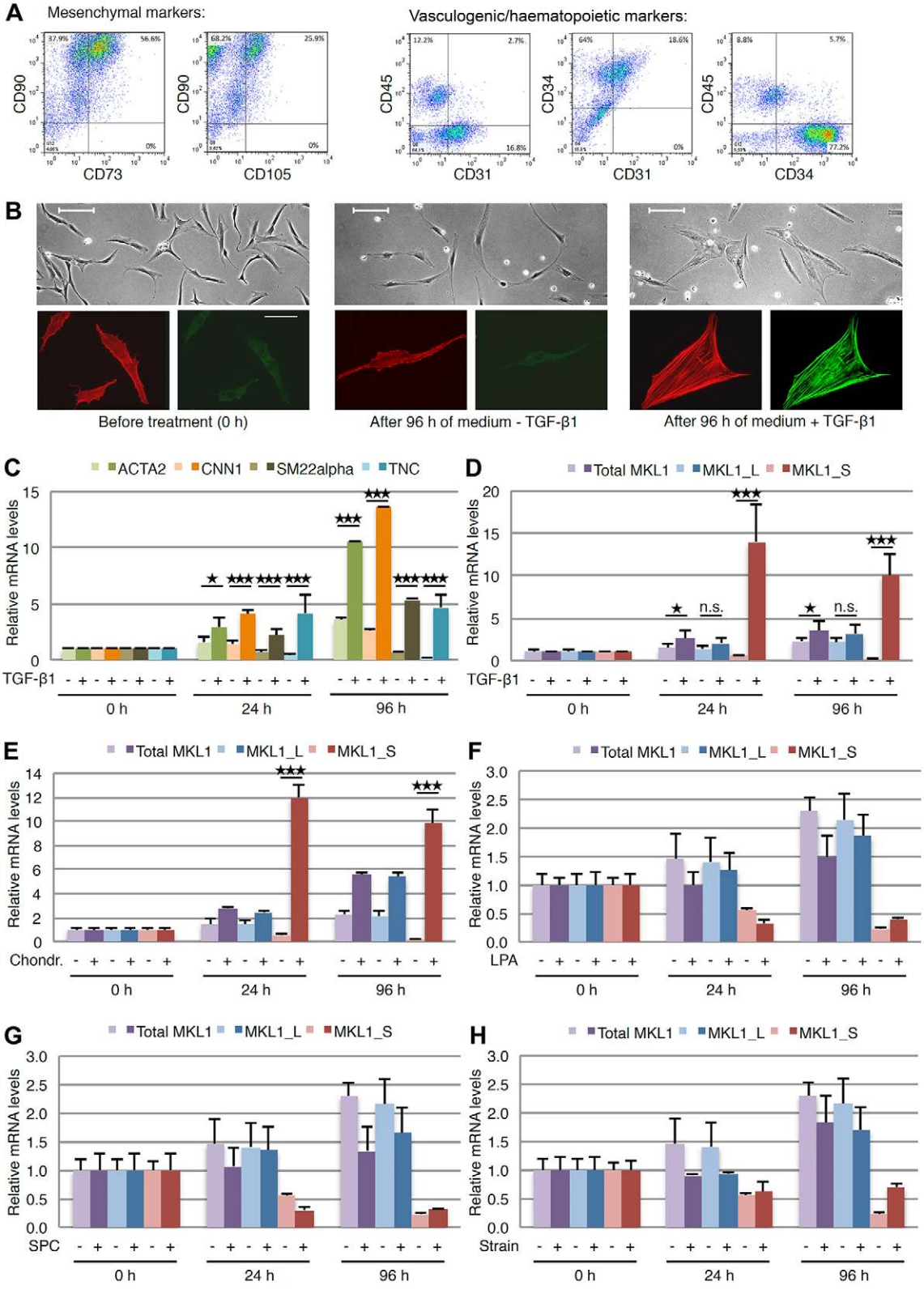

Fig. 4. Specific upregulation of MKL1_S during the initial phase of TGF-β-induced myofibroblast differentiation. (A) Cytofluorimetric profile of the SVF from which the adherent hASC population was generated for the differentiation experiments. (B) Phase-contrast pictures of TGF-β1-induced differentiation of hASCs (top panel). Cells stained with phalloidin (red) and anti-SMA (green) are shown in bottom panels. Cells were starved and kept in serum-free medium with or without 2 ng/ml TGF-β1 for 96 h. Scale bars: 200 μm (top panels), 50 μm (bottom panels). (C) qPCR analysis of myofibroblast marker levels relative to GAPDH during the initial phase of TGF-β1-induced myofibroblast differentiation. (D–H) qPCR analysis of MKL1 isoform levels relative to GAPDH during the initial phase of myofibroblastic differentiation induced by (D) 2 ng/ml TGF-β1, (E) chondrogenic medium (chondr.) containing 10 ng/ml TGF-β1, (F) 5 μM LPA, (G) 2 μM SPC, and (H) 5% uniaxial cyclic strain at 1 Hz for the initial 24 h. Data in C–H are represented as mean±s.d. ($n=4$). *$P<0.05$, ***$P<0.001$, n.s., not significant (unpaired Student's *t*-test).

Journal of Cell Science

Journal of Cell Science (2014) 127, 1079–1091 doi:10.1242/jcs.142075

did not result in obvious changes of the transcript levels of total MKL1 or one of the MKL1 isoforms (Fig. 4G,H). Therefore, the observed strong and isoform-specific induction of MKL1_S expression within the initial phase of hASC differentiation seems to be a mechanism that is specifically triggered by TGF-β1.

MKL1_S activates a group of genes in an isoform-specific manner

To investigate possible consequences of MKL1_S induction during myofibroblast differentiation we analyzed MKL1_S-specific effects on gene transcription. Because it is impossible to select stable overexpression/knockdown clones from primary hASCs without the loss of their multipotent properties, we used a more easily tractable cell line that we found to react to MKL1 transfection with the induction of the myofibroblast marker *ACTA2* (SMA) for these experiments. We generated HEK293 cells stably overexpressing either of the two MKL1 isoforms (see Fig. 2D). To directly stimulate the Rho–actin–MKL1 pathway, we treated the cells with LPA and assessed MKL1-dependent gene regulation by gene expression profiling. The majority of genes that were significantly up- or down-regulated in the MKL1_S-overexpressing cells were comparably regulated by overexpression of MKL1_L. This group of common target genes contained *ACTA2* (SMA) and other genes that have been described previously as being direct targets of MKL1 or SRF (Table 1; supplementary material Table S1). The observation that both MKL1 isoforms seem to similarly induce SRF-dependent transcription is in agreement with the results from promoter–reporter assays shown above (Fig. 2E). However, our gene expression analysis revealed a group of genes that were differentially affected by the MKL1 isoform overexpression (Table 1; supplementary material Table S1). Within this group, most transcripts showed higher expression with MKL1_S than with MKL1_L overexpression. Some of these transcripts were more strongly inhibited by MKL1_L than by MKL1_S when compared to the empty vector control, which might point towards an increased inhibitory function of MKL1_L. Importantly, although MKL1_S was clearly less overexpressed than MKL_L compared to endogenous MKL1 levels in the empty vector control, several genes were significantly more strongly induced by MKL1_S. By contrast, only a single gene of the top ten differentially regulated genes was specifically upregulated by the MKL1_L isoform. Interestingly, several genes that code for extracellular proteins such as proteases (e.g. MMP16), MMP regulators (e.g. SPOCK3/testican-3) or ECM components (e.g. osteocrin/musclin) were specifically upregulated by MKL_S. MMP16 showed the strongest MKL1_S-specific upregulation. To test whether this transcriptional regulation also occurs during hASC differentiation, we analyzed MMP16 transcript levels during differentiation induced by TGF-β, LPA, SPC or cyclic strain. MMP16 levels were elevated after 96 h of TGF-β-induced myofibroblast differentiation, but downregulated compared to the medium control with all other stimuli (Fig. 5). This might reflect the effect of the TGF-β-mediated induction of MKL1_S transcript levels in myofibroblast differentiation, which could control MMP16 expression in a delayed fashion.

The specific MKL1_S transcriptional activity requires a novel N-terminal domain

The observations of a strong and partly specific transcriptional activity of MKL1_S and an increased suppressive effect of

Table 1. MKL1_S and MKL1_L overexpression induce a common and an MKL1_S-specific transcriptional activity.

Gene name	Description	MKL_S versus empty vector[a]	MKL_L versus empty vector[a]	MKL_S versus MKL_L[a]
Genes similarly regulated by the two isoforms:				
POM121L1P	POM121 membrane glycoprotein-like 1 pseudogene	+3.89 (2.6×10^{-4})	+5.83 (4.2×10^{-5})	<1.50
NAP1L3	Nucleosome assembly protein 1-like 3	+.2.78 (2.4×10^{-6})	+1.86 (1.0×10^{-4})	<1.50
ACTA2	Actin, alpha 2, smooth muscle	+2.02 (3.0×10^{-5})	+1.86 (7.2×10^{-5})	<1.50
ESRRG	Estrogen-related receptor gamma	+1.93 (4.5×10^{-8})	+1.71 (2.2×10^{-7})	<1.50
MDGA2	MAM domain containing GPI anchor 2	+1.83 (1.8×10^{-5})	+2.43 (9.4×10^{-7})	<1.50
DACH2	Dachshund homolog 2 (*Drosoph.*)	+1.82 (1.5×10^{-5})	+1.61 (8.0×10^{-5})	<1.50
SLC8A1	Solute carrier family 8 (sodium/calcium exchanger), member 1	+1.67 (1.7×10^{-5})	+2.18 (6.6×10^{-7})	<1.50
PDGFD	Platelet derived growth factor D	+1.61 (8.3×10^{-6})	+1.50 (2.6×10^{-5})	<1.50
ESRP1	Epithelial splicing regulatory protein 1	−4.20 (2.3×10^{-8})	−2.88 (2.6×10^{-7})	<1.50
IFI16	Interferon, gamma-inducible protein 16	−2.96 (2.3×10^{-7})	−3.35 (9.8×10^{-8})	<1.50
MEOX2	Mesenchyme homeobox 2	−2.62 (2.1×10^{-6})	−3.15 (5.5×10^{-7})	<1.50
PION	Pigeon homolog (*Drosophila*)	−2.48 (4.3×10^{-5})	−2.47 (4.4×10^{-5})	<1.50
LGALS8	Lectin, galactoside-binding, soluble, 8	−2.22 (1.1×10^{-4})	−2.43 (5.3×10^{-5})	<1.50
Genes differentially regulated by the two isoforms:				
MMP16	**Matrix metallopeptidase 16 (membrane-inserted)**	**+5.86 (1.4×10^{-7})**	**+2.30 (4.5×10^{-5})**	**+2.54 (2.0×10^{-5})**
SPOCK3	**Sparc/osteonectin, cwcv and kazal-like domains proteoglycan (testican) 3**	**+5.04 (8.5×10^{-9})**	**+2.31 (1.6×10^{-6})**	**+2.18 (2.7×10^{-6})**
OSTN	**Osteocrin (musclin)**	**+2.23 (3.5×10^{-5})**	**<1.20**	**+1.92 (1.6×10^{-4})**
ODZ1	Odz, odd Oz/ten-m homolog 1 (*Drosophila*)	−1.85 (2.6×10^{-5})	−3.55 (1.0×10^{-7})	+1.91 (1.8×10^{-5})
NRG3	Neuregulin 3	<1.20	−1.71 (1.5×10^{-5})	+1.70 (1.5×10^{-5})
AMBN	**Ameloblastin (enamel matrix protein)**	**+5.14 (2.0×10^{-7})**	**+3.09 (3.7×10^{-6})**	**+1.67 (1.0×10^{-3})**
ADAM21	**ADAM metallopeptidase domain 21**	**+1.38 (3.7×10^{-6})**	**−1.36 (8.4×10^{-4})**	**+1.65 (3.0×10^{-5})**
MAP7D2	MAP7 domain containing 2	−1.77 (3.8×10^{-6})	−2.77 (4.1×10^{-8})	+1.56 (2.5×10^{-5})
CNTN4	Contactin 4	<1.20	−1.72 (1.3×10^{-6})	+1.54 (8.3×10^{-6})
FABP6	Fatty acid binding protein 6	<1.20	+2.00 (7.7×10^{-7})	−1.78 (3.0×10^{-6})

[a]Averaged fold-regulations of genes are given with *P*-values in parentheses.
Genes that were specifically induced by MKL1_S are highlighted in bold.

Journal of Cell Science (2014) 127, 1079–1091 doi:10.1242/jcs.142075

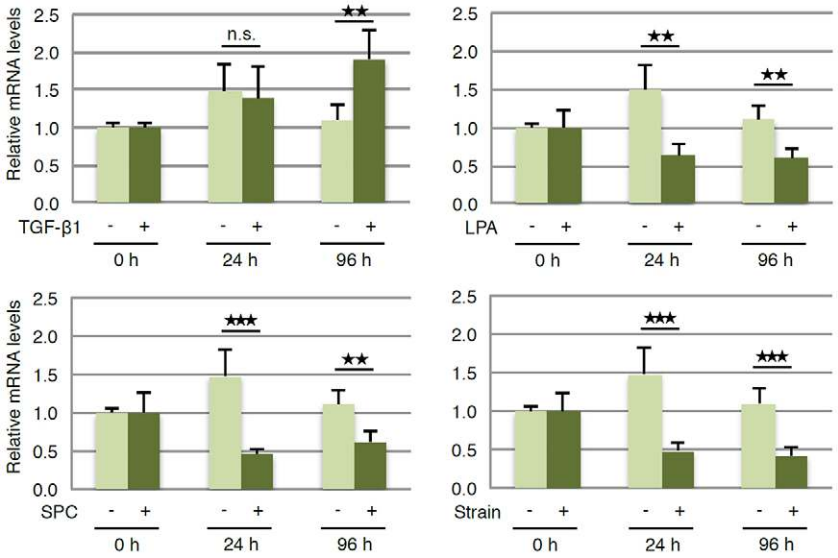

Fig. 5. MMP16 upregulation during myofibroblast differentiation. qPCR analysis of the MKL1_S target gene *MMP16* during the initial phase of hASC differentiation induced by 2 ng/ml TGF-β, 5 µM LPA, 2 µM SPC, or 5% uniaxial cyclic strain at 1 Hz for the initial 24 h. Levels are relative to GAPDH. Data are represented as mean±s.d. (n=4). $^{**}P<0.01$, $^{***}P<0.001$, n.s., not significant (unpaired Student's t-test).

MKL1_L led us to consider that their unique N-termini were responsible for these differential activities. Bioinformatical analyses of the N-terminal sequences, predicted that there is a 9-amino-acid transactivation domain (9aa TAD) within the specific 15 N-terminal amino acids (MAVQSVLQL) of MKL1_S. 9aa TADs have been described as the smallest known denominator in the transactivation domains of a variety of transcription factors, ranging from yeast to mammals (Martin, 2009; Piskacek et al., 2007). Owing to the fact that the border between the isoform-specific parts and the shared sequence lies within this motif, the corresponding sequence in MKL1_L (SERKNVLQL) does not fulfill the criteria for such a domain (Fig. 6A). Furthermore, secondary structure predictions (performed with CLC Main Workbench version 6.7) predicted a more extended α-helix upstream of the RPEL1 motif in MKL1_S than in MKL1_L (Fig. 6A). In addition to the predicted N-terminal 9aa TAD in MKL1_S, the algorithm detected another 9aa TAD in the C-terminal region that is common to both isoforms (DDLFDILIQ). This C-terminal region harbors the only MKL1 transactivation domain described so far. To test the hypothesis that the newly identified N-terminal motif in MKL1_S contributes to its specific transcriptional activity, we transfected HEK293 cells with different constructs containing altered or exchanged N-terminal motifs (Fig. 6B, see supplementary material Fig. S2 for expression of the translated proteins). After stimulation of the Rho–actin–MKL pathway by LPA treatment, we isolated RNA and analyzed the expression levels of the two MKL1_S-specific targets MMP16 and SPOCK3. Constructs missing the C-terminal half of MKL1, regardless of which N-terminal isoform sequence was used (MKL1_L_ΔC or MKL1_S_ΔC), did not support an increased MMP16 or SPOCK3 expression compared to empty-vector-transfected control cells (Fig. 6C). Thus, the activation of MKL1_S-specific target genes requires the C-terminal half of MKL1, including the C-terminal transactivation domain. Similar to what we observed in the gene expression profiling, overexpression of MKL1_S triggered MMP16 and SPOCK3 transcription 3- to 4-fold more efficiently than did overexpression of MKL1_L. However, when we mutated the predicted 9aa TAD in MKL1_S into a sequence that did not meet several of the criteria for 9aa TADs (KRGHSVLQL, MKL1_S 9aa mut), MMP16 and SPOCK3 expression dropped to roughly the level in MKL1_L-overexpressing cells. Moreover, when we exchanged this motif with the corresponding sequence of MKL1_L (MKL1_S 9aa_L), we observed the same drop of activity, suggesting that the identified motif in MKL1_S indeed confers higher activity towards certain target genes. However, we did not observe any enhancement of MKL1_L-mediated gene expression of MMP16 and SPOCK3 when we replaced its corresponding sequence with the functional domain of MKL1_S (MKL1_L 9aa_S) in the context of its long N-terminal tail. Furthermore, expression of a fusion construct between both isoforms (MKL1_L_S fusion), in which we fused the long N-terminal tail of MKL1_L to the N-terminus of MKL1_S, resulted in similarly low expression of MMP16 and SPOCK3. In summary, these results argue for a functional activating motif in MKL1_S when present in its natural context, as well as for a dominant inhibitory function of the MKL1_L-specific tail.

DISCUSSION

The Rho–actin–MKL1–SRF pathway has been implicated in several physiological and pathological processes based on the reversible differentiation of different precursor cell types into myofibroblasts (Small, 2012). Within this pathway, MKL1 activity has emerged as the crucial relay between the status of the actin cytoskeleton and the transcription of a substantial proportion of SRF target genes (Selvaraj and Prywes, 2004; Wang et al., 2002). Before our study, human MKL1 was either assumed to start at the first in-frame ATG/Met start codon (Wang et al., 2002), resulting in a protein missing the first conserved RPEL1 motif, or at an unusual CTG/Leu-92 start codon (Miralles et al., 2003). In our experiments, we found no evidence for either of these two translation starts. Instead, we provide experimental evidence for translation starting at the upstream unusual GTG/Val-100 codon. Thus, the published MKL1 transcript translates into a protein (MKL1_L) that is 100 amino acids longer than

Journal of Cell Science (2014) 127, 1079–1091 doi:10.1242/jcs.142075

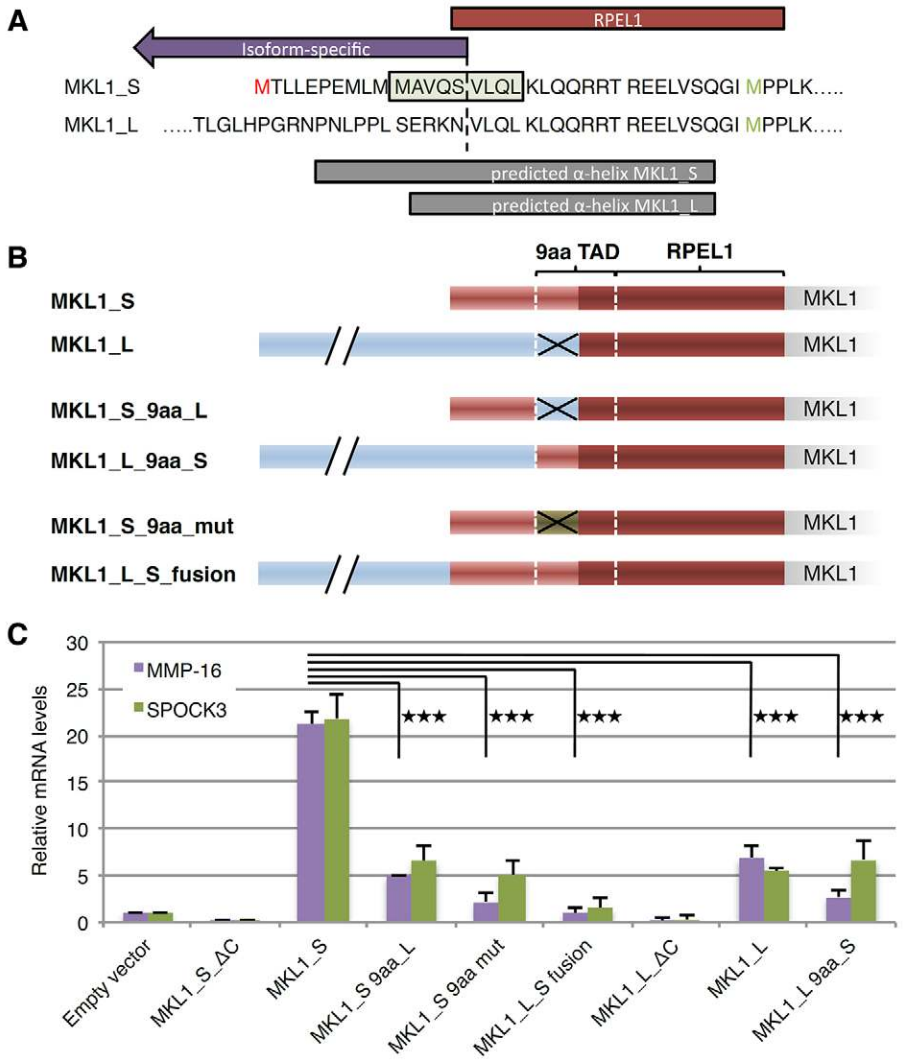

Fig. 6. Identification of a functional domain in MKL1_S that allows specific transcriptional activity. (A) Alignment of N-terminal amino acid sequences of the MKL1 isoforms. Green box, predicted 9aa TAD in MKL1_S; green letter, published ATG/Met start of MKL1_L; red letter, ATG/Met start of MKL1_S. (B) Schematic representations of the constructs used. A cross indicates a sequence that does not fulfill the 9aa TAD criteria. (C) qPCR analysis of MKL1_S-specific target genes. Constructs indicated were stably overexpressed in HEK293 cells. Before RNA extraction, cells were starved and MKL1 activity stimulated with LPA. MKL1_L and MKL1_S, 5′UTR-full-length constructs; ΔC constructs, MKL1 missing its C-terminal half. Data are represented as mean±s.d. of two independent experiments each with two independently created overexpressing cell lines ($n=4$). ***$P<0.001$ [MMP16 levels; one-way ANOVA (Holm–Sidak method)].

originally thought, and contains three actin-binding RPEL motifs. Compared to the suggested upstream CTG/Leu-92 codon, the novel GTG/Val-100 translation start includes eight more amino acids in the protein, which are predicted to form two short β-strands within a 4-β-strand motif at the MKL1_L N-terminus.

Moreover, we show for the first time that a second human MKL1 transcript variant arises from the utilization of an alternative promoter and is translated into the shorter MKL1_S. This isoform also contains three RPEL motifs, but a much shorter N-terminal domain than MKL1_L. In contrast to the MKL1_L transcript, which showed ubiquitous expression, we observed highly variable expression of the novel transcript, pointing towards more tissue-specific functions. Most studies published so far exclusively address total MKL1 levels using antibodies, PCR primers, or RNAi targeting the common part of the two MKL1 isoforms. Most studies based on overexpression of MKL1 constructs used either mouse MKL1_S, which was considered the major MKL1 protein in this species (Sasazuki et al., 2002; Wang et al., 2002), or engineered MKL1_L variants, with translation starts other than the GTG/Val-100 start. Therefore, some of the earlier findings on MKL1 function will have to be reevaluated with regard to the specific contributions of the two isoforms. Indeed, we found differential effects on gene expression by the two isoforms. In addition to a common transcriptional activity of MKL1_S and MKL1_L that included, for example, the regulation of SMA, the prototypic marker of the myofibroblast cell type, we identified a specific transcriptional activity of MKL1_S. We provide evidence that this activity is dependent on the initial five amino acids of a predicted 9aa TAD in the unique N-terminal stretch of MKL1_S. Appending the long N-terminal tail of MKL1_L to MKL1_S erased the MKL1_S-specific induction of its target genes MMP16 and SPOCK3. Thus, the presence of this large extension might interfere with the binding of an unknown factor to the predicted 9aa TAD. For instance, it has been suggested that this motif interacts with general transcriptional coactivators, such as the transcription initiation factor TFIID subunit 9 (TAF9) (Martin, 2009; Piskacek et al., 2007). Our experiments suggest a dual mode by which MKL1_L is disabled to induce certain MKL1_S target genes: (1) it is lacking the potential 9aa TAD, and (2) the presence of its long N-terminal tail has an inhibitory function.

In our study, we used primary hASCs as a differentiation model to study the two human MKL1 isoforms. In contrast to bone marrow, adipose tissue constitutes an easily accessible

Journal of Cell Science (2014) 127, 1079–1091 doi:10.1242/jcs.142075

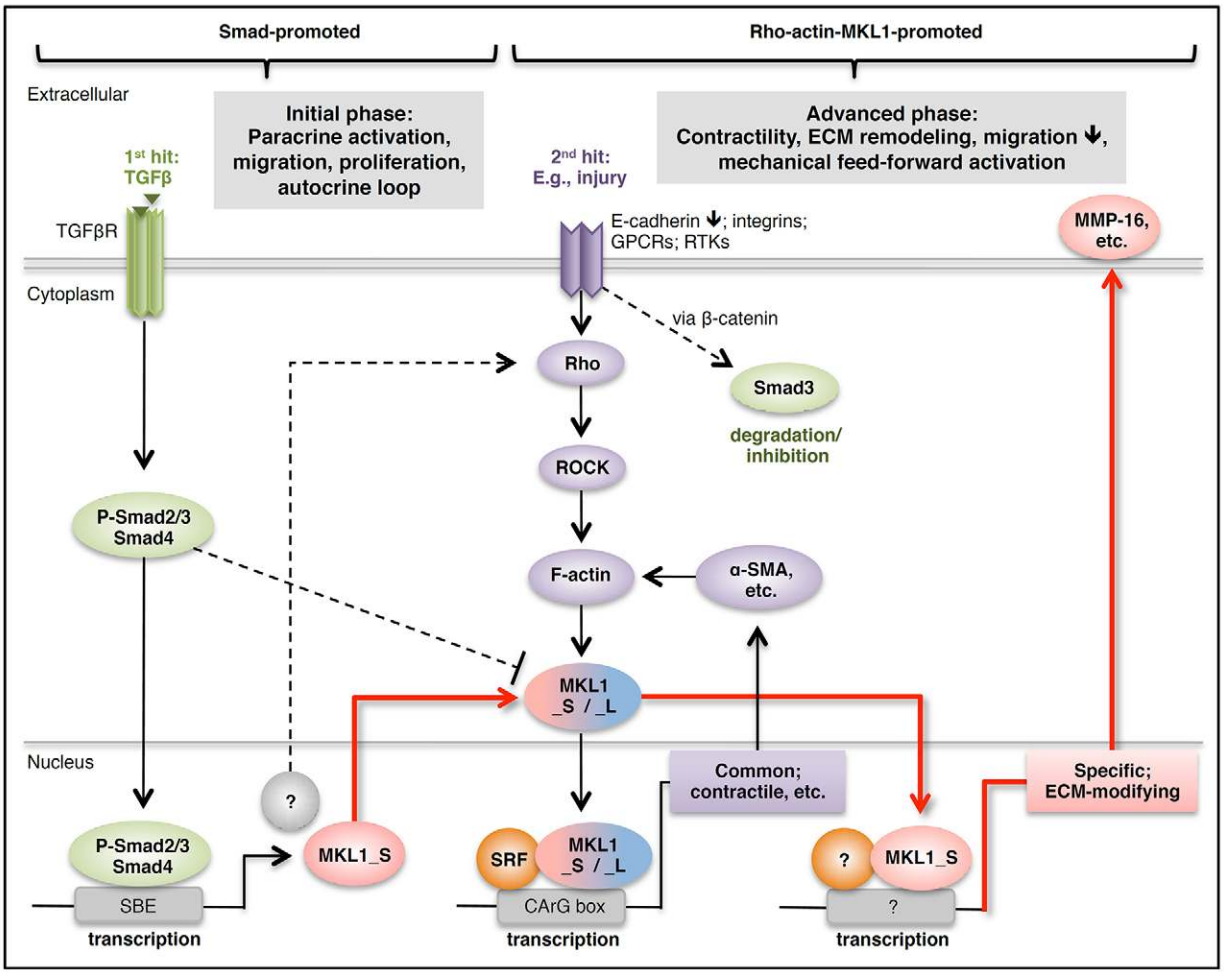

Fig. 7. Model for TGF-β-induced myofibroblast differentiation involving MKL1 isoform-specific activities. On the basis of the published models that seek to explain the delayed activation of the Rho–actin–MKL1 pathway by TGF-β during myofibroblast differentiation (Sandbo et al., 2011; Masszi et al., 2010), we propose that MKL1_S is one of the factors directly induced by Smad signaling during the initial phase of differentiation. Direct activation of the Rho–actin–MKL1 pathway by a second hit and/or the indirect activation via Smad signaling and MKL1_S induction are then likely to have two consequences. First, an SRF-mediated expression of contractile smooth-muscle-specific genes such as SMA, induced by either MKL1 isoform. Second, the expression of genes coding for ECM(-modifying) proteins regulated specifically by MKL1_S. We hypothesize that MKL1_S-specific transcription contributes to the progression to the advanced phase of myofibroblast differentiation involving ECM modifications and the downregulation of migration.

source for large numbers of patient-derived MSCs, which have an enormous potential for future applications in tissue regeneration (Zuk, 2010). Importantly, hASCs have been shown to differentiate into myofibroblasts and CAFs under the influence of tumor-secreted factors, such as TGF-β, and to promote the *in vitro* invasiveness of breast cancer cells (Jeon et al., 2010; Jotzu et al., 2011; Kakudo et al., 2012). We found that MKL1_S, but not MKL1_L, was strongly upregulated in primary hASCs within 24 h of TGF-β-induced myofibroblast differentiation. Consistently, we identified two putative Smad-binding elements (SBEs) in the MKL1_S proximal promoter region, but not for MKL1_L, making it likely that TGF-β-mediated Smad signaling directly induces transcription of MKL1_S. Current models suggest a complex interplay between TGF-β/Smad3 and the Rho–actin–MKL1 signaling pathways during myofibroblast differentiation (Charbonney et al., 2011; Masszi et al., 2010; Small, 2012). Several studies have shown that TGF-β upregulates total MKL1 expression and triggers the nuclear accumulation of MKL1, but not MKL2, in different precursor cells (Gupta et al., 2013; Mihira et al., 2012; Minami et al., 2012; Morita et al., 2007; Sandbo et al., 2011). However, TGF-β-mediated MKL1 translocation occurs in a delayed fashion compared to direct stimulation of the Rho–actin–MKL1 pathway. To explain the delayed activation, several models have been suggested that divide TGF-β-induced myofibroblast differentiation into different phases. Masszi and colleagues (Masszi et al., 2010) suggested that the direct induction of Smad signaling by TGF-β defines an early ‘Smad-promoted’ phase of the myofibroblast differentiation process in which Smad3 competes with SRF for binding to MKL1 and thus inhibits progression to the second phase (cf. Fig. 7). A two-step mechanism is supported by studies from Fan et al. (Fan et al., 2007) and Masszi et al. (Masszi et al., 2004) who found that for myofibroblastic differentiation of kidney tubular cells an epithelial cell injury is required as a second hit, which directly activates the Rho–actin–MKL1 pathway. Furthermore, Sandbo et al. (Sandbo et al., 2011) have proposed that TGF-β/Smad signaling induces the transcription of yet unknown factors that indirectly activate the Rho–actin–MKL1 pathway, thereby initiating the later phase of differentiation with a delay. We propose in our model that one of these unknown factors is

Journal of Cell Science (2014) 127, 1079–1091 doi:10.1242/jcs.142075

MKL1_S (Fig. 7). As a result of its induction, the generally low MKL1_S:MKL1_L ratio is raised substantially. Our gene expression analyses suggest that this results in MKL1_S-specific transcription of genes coding for extracellular proteins, including ECM proteins, proteases and MMP regulators. In addition to SRF-dependent contractile protein expression, which seems to be similarly induced by both MKL1 isoforms, the MKL1_S-specific gene regulation is likely to contribute to myofibroblast-mediated modification of the ECM. The protein products of *MMP16* and *SPOCK3*, the genes with the strongest MKL1_S-specific upregulation, are both known to regulate MMP2 activity (Nakada et al., 2001). The pro-migratory gene *MMP2* has been found to be downregulated by TGF-β in the later phase of fibroblast transformation into myofibroblasts (Howard et al., 2012). Furthermore, MMP2 is known to cleave latent TGF-β during the activation process of TGF-β from the ECM (Yu and Stamenkovic, 2000). Thus, MKL1_S might control the activation of MMP2 and in this way influence the motility of myofibroblasts, or their feed-forward activation via mechanical release of latent TGF-β from the ECM and its subsequent activation by MMP2.

The myofibroblast has emerged as a major target for anti-fibrotic therapies (Hinz et al., 2012). Remarkably, inhibition of the mechanosensitive Rho–actin–MKL1 pathway, for example, by genetic ablation of *MKL1*, was recently found to induce apoptosis in myofibroblasts and to inhibit experimental lung fibrosis (Zhou et al., 2013). Because of its specific and strong upregulation, the MKL1_S isoform has the potential to become a valuable biomarker for TGF-β-induced differentiation into myofibroblasts. Here, we reported the successful production of an antibody that specifically recognizes this isoform. Our findings also indicate that modulating MKL1-isoform-specific activities might become an important strategy in regenerative medicine, for example, for the engineering of myofibroblast- or smooth-muscle-like cells from hASCs. Furthermore, MKL1_S might become a novel target for the pharmacological intervention of persistent myofibroblast activation during fibrosis and cancer.

MATERIALS AND METHODS

MKL1 plasmid constructs and expression of recombinant MKL1 variants

The published human MKL1 cDNA (NM_020831) was amplified from total RNA from fetal human brain (AMS Biotechnology) and cloned into the pcDNA3.1 expression vector (Life Technologies). This sequence, termed 5′UTR-full length MKL1_L, comprises the full 5′UTR region and ends at the published stop codon (nucleotide position 3388, NM_020831). From this, ΔN-MKL1 was designed starting with the published ATG translation initiation codon (position 593, NM_020831). For MKL1_S, the 5′UTR sequence was amplified by 5′RACE experiments on total RNA from fetal (male, 24 weeks of age) and adult (male, 24 years of age) human brain (AMS Biotechnology) using the 5′/3′ RACE kit, 2nd generation (Roche). Reverse MKL1-specific primers SP1, SP2 and SP3 were designed to anneal to the published human *MKL1* mRNA downstream of the published ATG translation start (supplementary material Table S2). The novel MKL1_S 5′UTR (see supplementary material Fig. S1) was fused to the ΔN-full-length MKL1 construct resulting in the 5′UTR-full-length MKL1_S construct. The sequence of MKL1_S has been deposited in the European Nucleotide Archive at http://www.ebi.ac.uk/ena/data/view/HG764171). All ΔC constructs finish at nucleotide position 1984 of NM_020831. For MKL1_L_S fusion, the 5′ sequence of MKL1_L was fused to the MKL1_S-isoform-coding sequence starting with the first in-frame ATG. In the MKL1_S 9aa_L and the MKL1_L 9aa_S constructs the predicted 9aa TAD in MKL1_S (MAVQSVLQL) was exchanged with the corresponding sequence of MKL1_L (SERKNVLQL) or vice versa. For MKL1_S 9aa mut, the predicted 9aa TAD was mutated to KRGHSVLQL, which does not meet the 9aa TAD criteria (Piskacek et al., 2007). Site-directed mutagenesis was performed as described in Zheng et al. (Zheng et al., 2004). For the expression of recombinant MKL1 variants, HEK293 cells (EcR293 variant, Life Technologies/Invitrogen) were cultured at 37℃ and under 6% CO_2 in Dulbecco's Modified Eagle Medium (D-MEM; Seromed) containing 10% fetal calf serum (FCS; Life Technologies/Gibco). Cells were transfected using jetPEI™ (Polyplus-transfection SA). For stable overexpression, transfected cells were selected with 800 µg/ml G-418 (Roche) and pooled clones were cultured with 200 µg/ml G-418.

Antibodies and immunoblotting

Monoclonal antibodies (mAbs) were generated as described previously (Maier et al., 2008). For the isoform-specific 'anti-MKL1_S mAb', rats were immunized with a peptide comprising the 15 unique amino acids of human MKL1_S (MTLLEPEMLMMAVQS). For the 'anti-MKL1 total mAb', mice were immunized with a 6×His-tagged 19.5-kDa peptide comprising amino acids 215–395 of human MKL1 (NP_065882.1, NM_020831.3) that had been expressed in *E. coli* and purified by using ProBond nickel-chelating resin beads (Life Technologies/Invitrogen). Monoclonal antibodies were purified from cell culture supernatants via Protein-G–Sepharose-4 Fast Flow (GE Healthcare) following the manufacturer's instructions. A polyclonal 'anti-MKL1 total pAb' antibody was generated at Harlan Laboratories Ltd. Anti-β-tubulin antibody was from Sigma Aldrich. For immunoblotting, whole-cell extracts or purified protein solutions were separated on NuPAGE 4–12% Bis-Tris gels (Life Technologies/Invitrogen) and transferred onto a BioTrace PVDF membrane (PALL LifeSciences). After blocking with Odyssey Blocking Buffer (LI-COR Biosciences), primary antibodies were applied overnight at 4℃. Goat Alexa-Fluor-680-conjugated secondary antibodies against mouse or rat (Molecular Probes/Life Technologies) and donkey anti-rabbit IRDye 800 (Rockland) were applied for 1.5 h at room temperature (RT) and visualized with the Odyssey Imaging System (LI-COR Biosciences).

Affinity purification of MKL1 and Mass Spectrometry

Purified antibodies were coupled to $CNBr^-$-activated Sepharose beads 4B (GE Healthcare) according to the manufacturer's instructions. The affinity column was washed with three cycles of elution buffer (0.2 M Glycine-HCl, pH 3) and loading buffer (TST buffer, 50 mM Tris-HCl pH 7.6, 150 mM NaCl and 0.05% Tween 20). Whole-cell extracts were prepared in lysis buffer (50 mM Hepes pH 7.5, 140 mM NaCl, 1% Triton X-100 and Roche Complete Inhibitor Cocktail) and applied to the column overnight at 4℃ (diluted with an equal amount of loading buffer). Eluted protein-containing fractions were pooled, trichloro-acetic-acid-precipitated and resuspended in Laemmli buffer with 100 mM DTT. Cysteine residues were alkylated with 200 mM iodoacetamide before separation via SDS-PAGE. Protein bands were excised, washed with 25 mM NH_4HCO_3 and twice with 25 mM NH_4HCO_3 and acetonitrile (1:1), and digested with 100 ng endoproteinase AspN (Roche) overnight at 37℃. Peptides were analyzed by liquid chromatography mass spectrometry (LTQ Orbitrap Velos, Thermo Fisher Scientific).

Cell cultures and qPCR analysis and promoter reporter assay

RCH-ACV leukemia cells and epithelial bladder 5637 cells were obtained from the German Collection of Microorganisms and Cell Cultures. HeLa Cells were obtained from the European Cell Collection, Porton Down, UK. U343MG, U373, T98G and LN319 cells were kindly provided by Brian Hemmings (Friedrich Miescher Institute, Basel, Switzerland). These cell lines were maintained at 37℃ and under 6% CO_2 in D-MEM containing 10% FCS. Primary lung fibroblasts and airway smooth muscle cells were established from non-diseased peripheral lung tissue samples obtained from patients undergoing lung resection following approval by the ethics committee (kindly provided by Katrin E. Hostettler-Haack, Clinic of Respiratory Medicine, University Hospital Basel, Switzerland). Primary cells were grown in RPMI 1640

medium (Cambrex Bio Science) supplemented with 10% FCS and 1% MEM-vitamins (Cambrex Bio Science).

The pSRE-SEAP reporter assay was performed in transiently transfected HEK293 cells as described previously (Asparuhova et al., 2011).

Total RNA from cultured cells was extracted using the RNeasy and QiaShredder kits (Qiagen) and transcribed into cDNA using the High Capacity cDNA Reverse Transcription kit (Life Technologies/Applied Biosystems) with random primers. Relative quantification (ΔΔCt method) or Relative Standard Curve quantification was performed using the SYBR qPCR Supermix W/ROX from Invitrogen/Life Technologies and human *GAPDH* as internal reference gene. Intron-spanning primers including variant-specific exon–exon-spanning primers were designed for each MKL1 isoform and for MKL1 total (see supplementary material Table S2 for primer sequences). Experiments were performed on the StepOnePlus™ Real-Time PCR system (Life Technologies/Applied Biosystems).

Stem cell isolation from human adipose tissue

Adipose tissue in the form of liposuction was obtained from a healthy donor following informed consent and according to a protocol approved by the local ethical committee (EKBB, Ref. 78/07). The donor was male and younger than 20 years of age. Liposuction samples were digested with 0.075% collagenase type II (355 U/mg, Worthington) for 60–90 min at 37℃. After centrifugation, the cellular pellet was washed once with PBS (Life Technologies/Gibco). Red blood cells were lysed by incubation in ammonium chloride solution following the manufacturer's protocol (Stemcell Technologies). The resulting SVF cells were then resuspended in α-MEM (Life Technologies/Gibco) containing 10% FCS, 1 mM sodium pyruvate, 10 mM HEPES buffer, 100 U/ml penicillin, 100 µg/ml streptomycin and 0.29 mg/ml L-glutamate (complete medium, CM) (all from Life Technologies/Gibco). For monolayer expansion, 3.5×10^3 cells/cm^2 were seeded onto tissue culture plates, cultured in CM supplemented with 5 ng/ml FGF-2 (R&D Systems), and serially replated when reaching subconfluence. The expanded adipose-derived cells are referred to as hASCs. To verify the presence of a mesenchymal population, cells were incubated for 30 min with antibodies against the mesenchymal markers CD105 (FITC-conjugated, Serotec), CD90 (FITC-conjugated, BD Bioscience) and CD73 (APC-conjugated, BD Bioscience) and against the endothelial markers CD45, CD31 and CD34 (FITC-, PE- and APC-conjugated, respectively; all from BD Bioscience), and analyzed with a flow cytometer (FACSCalibur, BD Bioscience).

hASC differentiation

hASCs between passage numbers 1 and 3 were plated at a density of 3.5×10^3 cells/cm^2, starved the next day for 20 h in serum-free α-MEM, and cultured in serum-free α-MEM substituted with 2 ng/ml human TGF-β1 (R&D Systems), 2 µM sphingosylphosphorylcholine (SPC), or 5 µM Oleoyl-α-lysophosphatidic acid (LPA) (both Sigma-Aldrich) for 24 or 96 h. For differentiation into chondrocytes, hASCs were plated at a density of 1.5×10^4 cells/cm^2, starved for 20 h, and cultured in chondrogenic medium (D-MEM supplemented with ITS^{+1}, Sigma-Aldrich), 0.1 mM ascorbic acid 2-phosphate, 1.25 mg/ml human serum albumin, 1×10^{-7} M dexamethasone and 10 ng/ml TGF-β1) for 24 or 96 h. For mechanically induced hASC differentiation, hASCs were seeded at a density of 3.5×10^3 cells/cm^2 on flexible silicone membranes coated with fibronectin (BioFlex® 6-well culture plates; Flexcell International) as described previously (Chiquet et al., 2004; Maier et al., 2008). Cells were starved for 20 h in serum-free α-MEM before applying 5% equibiaxial cyclic strain at 1 Hz for 24 h using a computer-controlled vacuum system (Flexcell FX-4000; Flexcell International). Transcript levels were measured either directly (24 h timepoint), or after 72 h in serum-free α-MEM (96 h timepoint).

Immunofluorescence staining and nuclear translocation assays

HEK293 cells overexpressing MKL1 variants were grown on poly-L-lysine-precoated four-compartment plastic tissue culture dishes (Greiner Bio-One) and, after starvation in serum-free D-MEM for 20 h, stimulated with 2 µM Cytochalasin D (Calbiochem), 50 µM LPA (Sigma-Aldrich), or 15% FCS. Cells were fixed with 4% paraformaldehyde for 20 min and permeabilized with 0.1% Triton X-100 for 5 min before staining with anti-MKL1 total mAb and goat anti-mouse conjugated to Alexa Fluor 568 (Invitrogen/Life Technologies). MKL1-expressing cells were classified according to their predominant MKL1 localization into 'nuclear', 'pancellular' or 'cytosolic'.

For preparation of cytoplasmic and nuclear extracts, cells were lysed by incubation in 10 mM HEPES pH 7.9, 100 mM KCl, 1 mM EDTA, 1 mM DTT and 0.5% NP-40 for 5 min at 4℃, mixed vigorously and centrifuged at 5000 rpm at 4℃. The supernatant was collected as cytoplasmic extract. The nuclear pellets were washed with lysis buffer lacking NP-40, resuspended in 250 mM Tris-HCl pH 7.8, 100 mM KCl, 1 mM EDTA, 1 mM DTT, 0.5% NP-40 and 20% glycerol and vigorously shaken at 4℃ for 1 h. After centrifugation at 10,000 rpm for 30 min at 4℃, the nuclear extract was collected and, together with the cytoplasmic extract, used for 10% SDS-PAGE, followed by transfer onto a PVDF membrane and immunoblotting using the anti-MKL1 total mAb, anti-lamin A/C (BD Biosciences) and anti-GAPDH (Abcam) antibodies. After incubation with the appropriate horseradish-peroxidase-conjugated secondary antibodies (MP Biomedicals), SuperSignal West Dura Chemiluminescent Substrate (ThermoFisher Scientific) was used for detection.

DNA microarray analysis

HEK293 cells constitutively expressing: condition 1, the empty pcDNA3.1 vector; condition 2, the 5′UTR-full-length MKL_L construct, or condition 3, the 5′UTR-full-length MKL_S construct were grown in triplicates until they reached 70% confluence. Cells were starved for 16 h in D-MEM/0.3% FCS and treated with 50 µM LPA for 4 h. Total RNA was extracted using the RNeasy and QiaShredder kits (Qiagen). RNA was converted into labeled sense-strand cDNA with the Ambion WT expression kit (Life Technologies) and hybridized to Affymetrix Human Gene 1.0 arrays (Affymetrix) with a hybridization time of 16 h. Raw data were normalized using robust multi-array average (RMA), as implemented in the Bioconductor 2.15 package affy. Differentially expressed genes with a minimum average expression value of 4.0 ($\log_2$) were identified using the empirical Bayes method (*F* test) implemented in the limma package from Bioconductor. Contrasts were calculated for condition 2 versus condition 1, condition 3 versus condition 1, and condition 3 versus condition 2 with a non-adjusted *P*-value threshold of 0.001 (with Benjamini–Hochberg false discovery correction) and a minimum absolute linear fold change difference of 1.5.

Statistical analysis

Data are represented as stated in the figure legends. Student's *t*-tests were used for comparing two groups and one-way ANOVA (Holm–Sidak method) when comparing several groups. Statistical analysis was performed using SigmaPlot for Windows Version 12.0. Stars indicate statistical significance with $*P<0.05$; $**$ $P<0.01$; $***$ $P<0.001$; and n.s., not significant.

Acknowledgements

We thank Tim Roloff and his team from the Functional Genomics Facility of the Friedrich Miescher Institute for their help with the transcript profiling, Matthias Chiquet (University of Bern, Switzerland) and Richard P. Tucker (University of California Davis, USA) for critical reading of the manuscript and Maria Asparuhova (Friedrich Miescher Institute, Basel, Switzerland) for advice with cell fractionation.

Competing interests

The authors declare no competing interests.

Author contributions

M.A.S. designed and performed experiments, analyzed data and wrote the paper; B.E.P., R.S., D.Z. and J.F. designed and performed experiments. S.S. and I.M. developed analytical tools, and R.C.E. designed experiments, analyzed data and wrote the paper.

Funding

This work was supported by the Swiss National Science Foundation [grant numbers 31003A-120235 and 31003A-135584 to R.C.E.]; and the European

Community's Seventh Framework Programme [MultiTERM, grant agreement nr 238551 to B.E.P]. Deposited in PMC for immediate release.

Supplementary material

Supplementary material available online at
http://jcs.biologists.org/lookup/suppl/doi:10.1242/jcs.142075/-/DC1

References

Asparuhova, M. B., Ferralli, J., Chiquet, M. and Chiquet-Ehrismann, R. (2011). The transcriptional regulator megakaryoblastic leukemia-1 mediates serum response factor-independent activation of tenascin-C transcription by mechanical stress. *FASEB J.* **25**, 3477-3488.

Charbonney, E., Speight, P., Masszi, A., Nakano, H. and Kapus, A. (2011). β-catenin and Smad3 regulate the activity and stability of myocardin-related transcription factor during epithelial-myofibroblast transition. *Mol. Biol. Cell* **22**, 4472-4485.

Chiquet, M., Sarasa-Renedo, A. and Tunç-Civelek, V. (2004). Induction of tenascin-C by cyclic tensile strain versus growth factors: distinct contributions by Rho/ROCK and MAPK signaling pathways. *Biochim. Biophys. Acta* **1693**, 193-204.

Crider, B. J., Risinger, G. M., Jr, Haaksma, C. J., Howard, E. W. and Tomasek, J. J. (2011). Myocardin-related transcription factors A and B are key regulators of TGF-β1-induced fibroblast to myofibroblast differentiation. *J. Invest. Dermatol.* **131**, 2378-2385.

Fan, L., Sebe, A., Péterfi, Z., Masszi, A., Thirone, A. C., Rotstein, O. D., Nakano, H., McCulloch, C. A., Szászi, K., Mucsi, I. et al. (2007). Cell contact-dependent regulation of epithelial-myofibroblast transition via the rho-rho kinase-phospho-myosin pathway. *Mol. Biol. Cell* **18**, 1083-1097.

Gupta, M., Korol, A. and West-Mays, J. A. (2013). Nuclear translocation of myocardin-related transcription factor-A during transforming growth factor beta-induced epithelial to mesenchymal transition of lens epithelial cells. *Mol. Vis.* **19**, 1017-1028.

Hinz, B., Phan, S. H., Thannickal, V. J., Prunotto, M., Desmoulière, A., Varga, J., De Wever, O., Mareel, M. and Gabbiani, G. (2012). Recent developments in myofibroblast biology: paradigms for connective tissue remodeling. *Am. J. Pathol.* **180**, 1340-1355.

Howard, E. W., Crider, B. J., Updike, D. L., Bullen, E. C., Parks, E. E., Haaksma, C. J., Sherry, D. M. and Tomasek, J. J. (2012). MMP-2 expression by fibroblasts is suppressed by the myofibroblast phenotype. *Exp. Cell Res.* **318**, 1542-1553.

Jeon, E. S., Moon, H. J., Lee, M. J., Song, H. Y., Kim, Y. M., Cho, M., Suh, D.-S., Yoon, M.-S., Chang, C. L., Jung, J. S. et al. (2008a). Cancer-derived lysophosphatidic acid stimulates differentiation of human mesenchymal stem cells to myofibroblast-like cells. *Stem Cells* **26**, 789-797.

Jeon, E. S., Park, W. S., Lee, M. J., Kim, Y. M., Han, J. and Kim, J. H. (2008b). A Rho kinase/myocardin-related transcription factor-A-dependent mechanism underlies the sphingosylphosphorylcholine-induced differentiation of mesenchymal stem cells into contractile smooth muscle cells. *Circ. Res.* **103**, 635-642.

Jeon, E. S., Heo, S. C., Lee, I. H., Choi, Y. J., Park, J. H., Choi, K. U., Park, Y., Suh, D. S., Yoon, M. S. and Kim, J. H. (2010). Ovarian cancer-derived lysophosphatidic acid stimulates secretion of VEGF and stromal cell-derived factor-1 alpha from human mesenchymal stem cells. *Exp. Mol. Med.* **42**, 280-293.

Jotzu, C., Alt, E., Welte, G., Li, J., Hennessy, B. T., Devarajan, E., Krishnappa, S., Pinilla, S., Droll, L. and Song, Y.-H. (2011). Adipose tissue derived stem cells differentiate into carcinoma-associated fibroblast-like cells under the influence of tumor derived factors. *Cell. Oncol. (Dordr.)* **34**, 55-67.

Kakudo, N., Kushida, S., Suzuki, K., Ogura, T., Notodihardjo, P. V., Hara, T. and Kusumoto, K. (2012). Effects of transforming growth factor-beta1 on cell motility, collagen gel contraction, myofibroblastic differentiation, and extracellular matrix expression of human adipose-derived stem cell. *Hum. Cell* **25**, 87-95.

Kozak, M. (1989). Context effects and inefficient initiation at non-AUG codons in eucaryotic cell-free translation systems. *Mol. Cell. Biol.* **9**, 5073-5080.

Kurpinski, K., Chu, J., Wang, D. and Li, S. (2009). Proteomic profiling of mesenchymal stem cell responses to mechanical strain and TGF-beta1. *Cell. Mol. Bioeng.* **2**, 606-614.

Maier, S., Lutz, R., Gelman, L., Sarasa-Renedo, A., Schenk, S., Grashoff, C. and Chiquet, M. (2008). Tenascin-C induction by cyclic strain requires integrin-linked kinase. *Biochim. Biophys. Acta* **1783**, 1150-1162.

Martin, P. (2009). Common transactivation motif 9aaTAD recruits multiple general co-activators TAF9, MED15, CBP and p300. *Nature Precedings* **12**, 30.

Masszi, A., Fan, L., Rosivall, L., McCulloch, C. A., Rotstein, O. D., Mucsi, I. and Kapus, A. (2004). Integrity of cell-cell contacts is a critical regulator of TGF-beta 1-induced epithelial-to-myofibroblast transition: role for beta-catenin. *Am J. Pathol.* **165**, 1955-1967.

Masszi, A., Speight, P., Charbonney, E., Lodyga, M., Nakano, H., Szászi, K. and Kapus, A. (2010). Fate-determining mechanisms in epithelial-myofibroblast transition: major inhibitory role for Smad3. *J. Cell Biol.* **188**, 383-399.

Mihira, H., Suzuki, H. I., Akatsu, Y., Yoshimatsu, Y., Igarashi, T., Miyazono, K. and Watabe, T. (2012). TGF-β-induced mesenchymal transition of MS-1 endothelial cells requires Smad-dependent cooperative activation of Rho signals and MRTF-A. *J. Biochem.* **151**, 145-156.

Minami, T., Kuwahara, K., Nakagawa, Y., Takaoka, M., Kinoshita, H., Nakao, K., Kuwabara, Y., Yamada, Y., Yamada, C., Shibata, J. et al. (2012). Reciprocal expression of MRTF-A and myocardin is crucial for pathological vascular remodelling in mice. *EMBO J.* **31**, 4428-4440.

Miralles, F., Posern, G., Zaromytidou, A.-I. and Treisman, R. (2003). Actin dynamics control SRF activity by regulation of its coactivator MAL. *Cell* **113**, 329-342.

Morita, T., Mayanagi, T. and Sobue, K. (2007). Dual roles of myocardin-related transcription factors in epithelial mesenchymal transition via slug induction and actin remodeling. *J. Cell Biol.* **179**, 1027-1042.

Nakada, M., Yamada, A., Takino, T., Miyamori, H., Takahashi, T., Yamashita, J. and Sato, H. (2001). Suppression of membrane-type 1 matrix metalloproteinase (MMP)-mediated MMP-2 activation and tumor invasion by testican 3 and its splicing variant gene product, N-Tes. *Cancer Res.* **61**, 8896-8902.

Piskacek, S., Gregor, M., Nemethova, M., Grabner, M., Kovarik, P. and Piskacek, M. (2007). Nine-amino-acid transactivation domain: establishment and prediction utilities. *Genomics* **89**, 756-768.

Sandbo, N., Lau, A., Kach, J., Ngam, C., Yau, D. and Dulin, N. O. (2011). Delayed stress fiber formation mediates pulmonary myofibroblast differentiation in response to TGF-β. *Am. J. Physiol.* **301**, L656-L666.

Sarrazy, V., Billet, F., Micallef, L., Coulomb, B. and Desmoulière, A. (2011). Mechanisms of pathological scarring: role of myofibroblasts and current developments. *Wound Repair Regen.* **19 Suppl. 1**, s10-s15.

Sasazuki, T., Sawada, T., Sakon, S., Kitamura, T., Kishi, T., Okazaki, T., Katano, M., Tanaka, M., Watanabe, M., Yagita, H. et al. (2002). Identification of a novel transcriptional activator, BSAC, by a functional cloning to inhibit tumor necrosis factor-induced cell death. *J. Biol. Chem.* **277**, 28853-28860.

Selvaraj, A. and Prywes, R. (2004). Expression profiling of serum inducible genes identifies a subset of SRF target genes that are MKL dependent. *BMC Mol. Biol.* **5**, 13.

Small, E. M. (2012). The actin-MRTF-SRF gene regulatory axis and myofibroblast differentiation. *J. Cardiovasc. Transl. Res.* **5**, 794-804.

Tomasek, J. J., Gabbiani, G., Hinz, B., Chaponnier, C. and Brown, R. A. (2002). Myofibroblasts and mechano-regulation of connective tissue remodelling. *Nat. Rev. Mol. Cell Biol.* **3**, 349-363.

Wang, D., Chang, P. S., Wang, Z., Sutherland, L., Richardson, J. A., Small, E., Krieg, P. A. and Olson, E. N. (2001). Activation of cardiac gene expression by myocardin, a transcriptional cofactor for serum response factor. *Cell* **105**, 851-862.

Wang, D.-Z., Li, S., Hockemeyer, D., Sutherland, L., Wang, Z., Schratt, G., Richardson, J. A., Nordheim, A. and Olson, E. N. (2002). Potentiation of serum response factor activity by a family of myocardin-related transcription factors. *Proc. Natl. Acad. Sci. USA* **99**, 14855-14860.

Yu, Q. and Stamenkovic, I. (2000). Cell surface-localized matrix metalloproteinase-9 proteolytically activates TGF-beta and promotes tumor invasion and angiogenesis. *Genes Dev.* **14**, 163-176.

Zheng, L., Baumann, U. and Reymond, J.-L. (2004). An efficient one-step site-directed and site-saturation mutagenesis protocol. *Nucleic Acids Res.* **32**, e115.

Zhou, Y., Huang, X., Hecker, L., Kurundkar, D., Kurundkar, A., Liu, H., Jin, T.-H., Desai, L., Bernard, K. and Thannickal, V. J. (2013). Inhibition of mechanosensitive signaling in myofibroblasts ameliorates experimental pulmonary fibrosis. *J. Clin. Invest.* **123**, 1096-1108.

Zuk, P. A. (2010). The adipose-derived stem cell: looking back and looking ahead. *Mol. Biol. Cell* **21**, 1783-1787.